

Original Article

Cite this article: O'Sullivan GJ, Hoare BC, Mark C, Drakou F, and Tomlinson EL (2023) Uranium–lead geochronology applied to pyrope garnet with very low concentrations of uranium. *Geological Magazine* **160**: 1010–1019. <https://doi.org/10.1017/S0016756823000122>

Received: 26 July 2022

Revised: 10 February 2023

Accepted: 13 February 2023

First published online: 21 March 2023


Keywords:

pyrope; garnet; geochronology; mantle; kimberlite; diamond; geochemistry

Author for correspondence: Gary J O'Sullivan, Emails: gary.osullivan@ucd.ie; gjosulli@tcd.ie

*Now at: Department of Geosciences, Swedish Museum of Natural History, Stockholm, SE-104 05, Sweden

Uranium–lead geochronology applied to pyrope garnet with very low concentrations of uranium

Gary J O'Sullivan¹ , Brendan C Hoare², Chris Mark^{1,*}, Foteini Drakou³ and Emma L Tomlinson³

¹UCD School of Earth Sciences, University College Dublin, Dublin 4, Ireland; ²Geological Institute of America (GIA), New York, NY 10036, USA and ³Department of Geology, Trinity College Dublin, Dublin 2, Ireland

Abstract

We present U–Pb dates from peridotitic pyrope-rich garnet from four mantle xenoliths entrained in a kimberlite from Bultfontein, South Africa. Garnet dates magmatic emplacement due to the high mantle residence temperatures of the source material prior to eruption, which were most likely above the closure temperature for the pyrope U–Pb system. We determine a U–Pb date of 84.0 ± 8.1 Ma for the emplacement of the Bultfontein kimberlite from garnet in our four xenolith samples. The date reproduces previous dates obtained from other mineral–isotope systems (chiefly Rb–Sr in phlogopite). Garnet can be dated despite extremely low concentrations of U (median ~ 0.05 $\mu\text{g/g}$), because concentrations of common Pb are often low or non-detectable. This means that sub-concordant garnets can be dated with moderate precision using very large laser-ablation spots (130 μm) measured by quadrupole inductively coupled plasma – mass spectrometry (LA-Q-ICP-MS). Our strategy demonstrates successful U–Pb dating of a U-poor mineral due to high initial ratios of U to common Pb in some grains, and the wide spread of isotopic compositions of grains on a concordia diagram. In addition, the analytical protocol is not complex and uses widely available analytical methods and strategies. This new methodology has some advantages and disadvantages for dating kimberlite emplacement versus established methods (U-based decay systems in perovskite and zircon, or Rb- or K-based systems in phlogopite). However, this method has unique promise for its potential application to detrital diamond prospecting and, more speculatively, to the dating of pyrope inclusions in diamond.

1. Introduction

Dating of minerals by U–Pb geochronology traditionally targets U-rich minerals with concentrations of U in the single- to thousands-of- $\mu\text{g/g}$ range; examples include zircon, baddeleyite and rutile. U-rich minerals are attractive targets, as the ratio of Pb produced by radioisotope decay (radiogenic Pb) to Pb present when the mineral formed (common Pb) is typically high, providing precise ages. However, materials with low concentrations of U, but correspondingly low concentrations of common Pb, might also be dated if a suitable analytical procedure is used. Dating of garnet by U–Pb methods was first demonstrated in the late 1980s (Mezger *et al.* 1989; Jung & Mezger, 2003) using thermal ionization mass spectrometry (TIMS), but such dating is hampered by uncertainty over whether U is hosted within the garnet lattice or within inclusions (e.g. DeWolf *et al.* 1996). Modern spatially resolved analytical approaches (laser ablation) surmount this issue, and coupled with the greater availability of characterized garnet reference materials (e.g. Seman *et al.* 2017), large numbers of garnet grains can be analysed and inclusions reliably detected (e.g. Chen *et al.* 2021). Here, we demonstrate U–Pb dating of garnet on a rather extreme case: U-depleted pyrope garnet from kimberlite-hosted sub-cratonic lithospheric mantle xenoliths with very low concentrations of U, but high ratios of radiogenic to common Pb. U–Pb dating of mantle garnet is an appealing prospect. An abundant rock-forming phase in the mantle and common as a xenocrystic phase in kimberlites, it is easy to identify and can incorporate U (Galuskina *et al.*, 2010; Rák *et al.* 2011). Furthermore, it is chemically and mechanically robust at the Earth's surface (Morton & Hallsworth, 2007). Interaction of garnet with melt and/or fluid can result in a kelyphite reaction that consumes such garnet and will preclude U–Pb dating, although the products of this reaction may be dated by the $^{40}\text{Ar}/^{39}\text{Ar}$ method to yield emplacement dates for kimberlite (Philips *et al.* 2012).

Kimberlite-hosted garnet are most likely entrained at ambient lithospheric temperatures of $>1000^\circ\text{C}$, in excess of closure temperatures of the almandine–pyrope U–Pb system inferred from experimental studies ($>800^\circ\text{C}$; Mezger *et al.* 1989). Therefore, the determined garnet U–Pb age from mantle will most commonly relate to magmatic emplacement rather than garnet formation (cf. Li *et al.* 2022) or subsequent metasomatic alteration.

© The Author(s), 2023. Published by Cambridge University Press. This is an Open Access article, distributed under the terms of the Creative Commons Attribution licence (<http://creativecommons.org/licenses/by/4.0/>), which permits unrestricted re-use, distribution and reproduction, provided the original article is properly cited.



The materials analysed for this study come from peridotite xenoliths entrained in kimberlite, a volatile-rich, silica-poor ultramafic mantle-derived magma that is rapidly and violently erupted onto the Earth surface. Kimberlites are of scientific interest as they provide rare glimpses into the composition and evolution of the Earth's lithospheric mantle. Kimberlites transport mantle xenoliths and xenocrysts, and importantly diamond, to the surface, providing a wealth of information on the chemical, thermal and geodynamic evolution of the lithosphere. Kimberlite magma emplacement can constrain critical processes such as craton erosion, ancient plume activity, and the Earth's tectonic evolution and deep volatile cycles (e.g. Janney *et al.* 2010; Tappe *et al.* 2018b). Constraining kimberlite emplacement may also aid detrital diamond prospecting, and models of the genesis of plume-associated metallogenic provinces (Fiorentini *et al.* 2020).

1.a. Commonly used dating methods applied to kimberlites and mantle xenoliths

Most preserved kimberlites were emplaced during the Phanerozoic and there have been several periods of enhanced kimberlite magmatism (Tappe *et al.* 2018b; Heaman *et al.* 2019). Kimberlites are dated by a range of different methods, most commonly using U–Pb perovskite (Tappe & Simonetti, 2012; Sarkar *et al.* 2015) and U–Pb zircon (e.g. Davis, 1977; Sun *et al.* 2018), and more recently by (U/Th)–He of perovskite in kimberlite groundmass (e.g. Stanley & Flowers, 2016) and U–Pb dating of rutile overgrowths on ilmenite megacrysts entrained in kimberlite (Tappe *et al.* 2014). Comparatively, attempts to date kimberlitic ilmenite by the U–Pb method have not been successful (Noyes *et al.* 2011).

U–Pb dating has also been applied to magmatic andraditic garnet from within the kimberlite groundmass (Li *et al.* 2022). However, such garnet is rare in kimberlite, more commonly occurring in ultramafic lamprophyres and orangeites (Mitchell, 1995). For information on the occurrence of similar rocks in South Africa see Tappe *et al.* (2022). Rubidium–strontium and $^{40}\text{Ar}/^{39}\text{Ar}$ in phenocrystic phlogopite are also employed to date kimberlites and can yield precise determinations. However, despite advancements, even current state-of-the-art methods for dating of kimberlite do not always yield accurate and precise ages. U–Pb analysis of perovskite can be complicated by high common-Pb contents and the occurrence of multiple age populations (Griffin *et al.* 2014), though recent developments (including the measurement of ^{204}Pb) have surmounted the common-Pb problem (e.g. Tappe *et al.* 2018a). Despite these improvements, U–Pb perovskite is not useful for detrital prospecting, as it is unstable at Earth surface conditions and occasionally requires both mineral and whole-rock isotopic measurements to be made, precluding detrital measurements.

U–Pb dating of kimberlite zircon is complicated by the fact that zircon crystallization may predate kimberlite magmatism and thus preserve ages that predate emplacement by millions to several billions of years (e.g. Kinny *et al.* 1989; Zartman & Richardson, 2005; Hoare *et al.* 2021). (U/Th)–He dating applied to zircon and perovskite circumvents some sources of error in kimberlite dating by analysing a daughter product retained only at low temperatures; however, the system is susceptible to resetting by post-emplacement tectonomagmatic processes (Stanley & Flowers, 2016), and additionally may not always provide precise age constraints amongst other issues (see Reich *et al.* 2007).

To conclude, while phlogopite will remain the most commonly employed dating method in kimberlite, it is more susceptible to

alteration after emplacement than some other components (amongst other complicating factors, see Heaman *et al.* 2019). This means that application of the Rb–Sr and $^{40}\text{Ar}/^{39}\text{Ar}$ phlogopite methods is not always possible. Furthermore, many of the other described methods rely upon the occurrence of the mineral phase: e.g. zircon is only an accessory mineral in kimberlite. Therefore, a method to date kimberlite using a common rock-forming and physically robust mineral, such that dating can be applied to garnets in altered kimberlites and those in detrital settings, is desirable, providing a rationale for this paper.

1.b. Previous isotopic dating at Kimberley

We have analysed garnet from four peridotite xenoliths collected from the Bultfontein pans near Kimberley and garnet mineral separate (eclogitic) from Jagersfontein, South Africa (Fig. 1). Information about previous dating performed on these kimberlites is provided in Figure 1. The emplacement of the Bultfontein kimberlite has been previously dated by the Rb–Sr method, yielding dates of 90 ± 3 Ma (Allsopp & Barrett, 1975) and 85.6 ± 1.0 Ma (Smith *et al.* 1985) determined from kimberlite matrix phlogopite. Phlogopite from entrained mantle xenoliths yielded a date of 84 ± 0.9 Ma (Kramers & Smith, 1983). These ages are typical of Group-I kimberlites in the wider 'Kimberley cluster' (Allsopp & Barrett, 1975). U–Pb zircon ages from the Bultfontein kimberlite range from 83.8 Ma (xenolith-hosted zircon) to 91.2 Ma (kimberlite zircon) (Davis, 1977); however, no MSWD or errors were reported for those dates. Age estimates for emplacement of the Bultfontein kimberlite thus range between *c.* 83 and 93 Ma (e.g. Fitzpayne *et al.* 2020), though the most precise and well-documented estimates cluster around the younger part of the age range.

2. Materials

Garnet were analysed from four peridotite xenoliths prepared as 200 μm thick sections, and also from eclogitic (orange) garnet within heavy mineral separates (i.e. xenocrysts hosted in the kimberlite) mounted in epoxy. All peridotite xenoliths were collected from the Bultfontein pans (28.739155° S, 24.818094° E), spoils derived from mining of the Bultfontein kimberlite pipe in South Africa. Samples BSK064, CLA-51 and BP002 (Tomlinson *et al.* 2018) are from garnet harzburgite. CLA-13 is a typical coarse-grained granular garnet lherzolite (Fig. 2). All samples are Cr-rich and depleted in composition, with Mg# (Mg/Mg + Fe) values of 0.83–0.86. Xenoliths were selected on the basis of minimal secondary metasomatic alteration (phlogopite absent). Garnet crystals in section are *c.* 300–1500 μm in size (Fig. 2). Attempts to utilize the U–Pb system to date eclogitic garnet separate from the Jagersfontein kimberlite were unsuccessful, owing to extremely low U concentrations (even by the standards of this study, with *c.* 8 ng/g median U). This sample is excluded from graphical display and further discussion, as no meaningful information can be gleaned.

3. Methodology

Garnet were imaged using a Tescan TIGER MIRA3 Variable Pressure Field Emission Scanning Electron Microscope (FE-SEM). Cathodoluminescence (CL) detectors were used to detect the presence or absence of mineral inclusions. Major elements were collected using calibrated energy-dispersive X-ray spectroscopy (EDS) at the iCrag laboratory, Trinity College Dublin

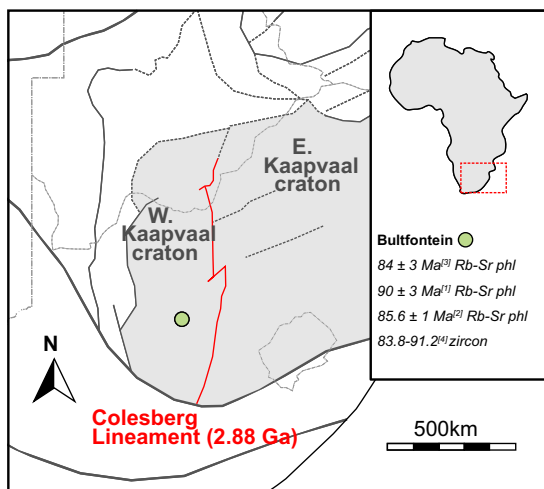


Fig. 1. (Colour online) Location of Bultfontein, where mantle xenoliths were sampled. Tectonic divisions of the Kaapvaal craton after Griffin *et al.* (2003). References in the key are [1] Allsopp & Barrett (1975); [2] Smith *et al.* (1985); [3] Kramers & Smith (1983); [4] Davis (1977); phl = phlogopite.

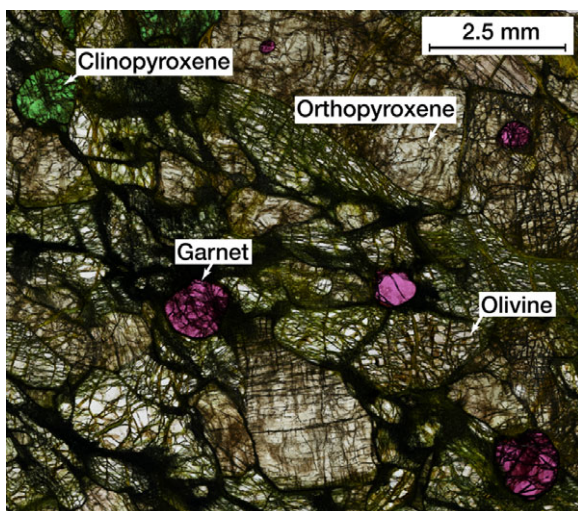


Fig. 2. (Colour online) Transmitted light image of a thick section of coarse-grained theralzite from Bultfontein (sample CLA-13). Garnet are magenta in colour.

(Table 1). The procedure for the SEM analysis is supplied in a supplementary file (Table S1). Garnet crystals were analysed for U–Pb isotopes by laser ablation – inductively coupled plasma mass spectrometry (LA-Q-ICP-MS) in the iCRAG laboratory at Trinity College Dublin. These data are also supplied in the supplementary file Table S1; the analytical settings are provided in Table 2.

A Teledyne-Cetac Analyte Excite 193 nm excimer laser, with a rapid-washout HelEx 2-volume ablation cell, was coupled via an in-house adjustable-volume signal smoothing device to an Agilent Technologies 7900 quadrupole ICP-MS. Masses ^{29}Si , ^{43}Ca , ^{137}Ba , ^{206}Pb , ^{207}Pb , ^{208}Pb , ^{232}Th and ^{238}U were monitored. ^{137}Ba was used to screen for contamination from kimberlite groundmass, with spots yielding significant baseline-corrected counts (>500 counts per second (CPS)) being excluded from age calculations (non-excluded grains had a median value of

~15 CPS ^{137}Ba). Calculated ages would likely be more precise if these ‘contaminated’ points were included, as they contain high counts on masses of Pb, but their inclusion could compromise the accuracy of the reported ages by distorting the calculated initial isotopic composition of discordia on a Tera–Wasserburg diagram. Excluded spots are listed in the supplementary U–Pb data (Supplementary Table S1).

^{29}Si was used as an internal standard to correct for variation in signal intensity. A large spot size of 130 μm diameter was used in order to optimize counts on U and Pb masses from the unknown garnets, while retaining reference material signal intensity well below the pulse-analogue threshold on this instrument (~ 10^7 CPS for isotopes of U and Pb). The low repetition rate (10 Hz), moderate fluence (2.1 J cm^{-2}) and large spot size (130 μm) used are in the range considered optimal for reducing matrix effects when analysing garnet for U–Pb (Chen *et al.* 2021). NIST614 standard glass was the primary standard for U–Pb and trace element analysis (Woodhead & Hergt, 2000). Data reduction employed the VizualAge data reduction scheme (DRS) for Iolite® (Paton *et al.* 2011; Petrus & Kamber, 2012), and for age calculations IsoplotR was used (Vermeesch, 2018). A U–Pb fractionation correction factor was obtained for each session from Odikhincha garnet (Salnikova *et al.* 2019; 250 ± 1 Ma) and applied to secondary references and garnet unknowns. Reported dates for unknown and secondary reference materials ages use $^{206}\text{Pb}/^{238}\text{U}$ vs $^{207}\text{Pb}/^{206}\text{Pb}$ ratios. Where possible, dates are reported from the lower intercept of discordia, including all unknowns. Where this is not possible, reported dates are calculated from the weighted mean of $^{206}\text{Pb}/^{238}\text{U}$ ratios.

The secondary reference materials Afrikanda garnet (Salnikova *et al.* (2019) TIMS age 378 ± 3 Ma; our ages, calculated from fractionation-corrected Tera–Wasserburg discordia lower intercept isotope ratios for session 1: 378 ± 7 Ma, MSWD = 2.6, $n = 12$; and session 2: 378 ± 4 Ma, MSWD = 1.7, $n = 12$), Dashkesan garnet (Stifeeva *et al.* (2019) TIMS age 147 ± 2 Ma; our fractionation-corrected weighted mean $^{206}\text{Pb}/^{238}\text{U}$ ages for session 1: 144.3 ± 1.3 Ma, MSWD = 1.7, $n = 11$; and session 2: 146.1 ± 1.3 Ma, MSWD = 0.84, $n = 7$) and Chikskii garnet (Salnikova *et al.* (2018) TIMS age 492 ± 2 Ma; our fractionation-corrected weighted mean $^{206}\text{Pb}/^{238}\text{U}$ ages for session 1: 492 ± 8 Ma, MSWD = 5.4, $n = 10$; and session 2: 478 ± 9 Ma, MSWD = 18, $n = 10$) were employed after U–Pb fractionation correction and treated in the same manner as the unknowns. Uncertainties are fully propagated and reported at the 2σ level here and throughout. In both sessions Chikskii garnet exhibited isotopic over-dispersion, demonstrated by its high MSWD. In session 2 this results in a mismatch between the published TIMS age and our age and renders ages unreliable. We reproduce the published TIMS ages of the other garnet secondary reference materials at the 2σ level. Mud Tank zircon (Black & Gulson, 1978: 736 ± 3 Ma; our session 1 concordia age 730.3 ± 2.6 Ma, MSWD = 1.6, $n = 14$; our session 2 concordia age 736.9 ± 3.9 Ma, MSWD = 0.56, $n = 14$) was analysed, without using a U–Pb correction factor. Details of our analytical protocol are provided in a supplementary document (Table S1). For Ni-in-garnet thermometry, ^{29}Si , ^{60}Ni , ^{90}Zr , ^{232}Th and ^{238}U were analysed in a separate session under the same analytical conditions as above with BHVO-2G as the primary reference material and BCR-2G employed as a secondary reference material (Jochum *et al.* 2005). For this experiment ^{29}Si was again used as the index mass. The Trace Elements DRS for Iolite® was used for data reduction (Paton *et al.* 2011).

Table 1. Representative major- (SEM-EDX) and trace-element (LA-Q-ICPMS) concentrations of garnet in Bultfontein xenoliths

(wt %)	BP002 (<i>n</i> = 11)	CLA-13 (<i>n</i> = 9)	CLA-51 (<i>n</i> = 19)	BSK064 (<i>n</i> = 12)
SiO ₂	41.97 ± 0.15	41.48 ± 0.13	41.83 ± 0.17	42.24 ± 0.12
TiO ₂	b.d.l ± b.d.l	b.d.l ± b.d.l	b.d.l ± b.d.l	b.d.l ± b.d.l
Al ₂ O ₃	21.22 ± 0.17	19.96 ± 0.11	19.88 ± 0.19	20.94 ± 0.16
Cr ₂ O ₃	3.82 ± 0.23	4.99 ± 0.10	5.23 ± 0.18	4.13 ± 0.20
MgO	21.35 ± 0.11	20.14 ± 0.13	21.04 ± 0.11	22.03 ± 0.11
FeO	6.43 ± 0.05	7.24 ± 0.05	6.70 ± 0.04	6.33 ± 0.04
MnO	0.24 ± 0.01	0.27 ± 0.02	0.25 ± 0.02	0.23 ± 0.01
CaO	4.66 ± 0.07	5.46 ± 0.05	5.30 ± 0.07	4.71 ± 0.06
Total	99.69	99.55	100.22	100.61
Ni (ppm)	41.0 ± 2.3	54.1 ± 3.2	40.3 ± 2.0	42.5 ± 1.0
Ni (°C)	971 ± 17	1057 ± 20	966 ± 15	981 ± 7
Zr (ppm)	67.6 ± 2.1	20.4 ± 5.7	59 ± 10	66.6 ± 1.6

Note: Sampling temperature estimates use the Ryan *et al.* (1996) Ni-in-Grt thermometer. Previous thermometry on sample BP002 (Tomlinson *et al.* 2018) using garnet–orthopyroxene Fe/Mg exchange thermometry yields a matching equilibration estimate of 975 °C (this study = 971 °C). Mg# = Mg/(Fe + Mg); Cr# = Cr/(Cr + Al); 'b.d.l.' = below detection limit; EDX = Energy-dispersive X-ray spectroscopy.

4. Results

Garnet have very low U–Th–Pb concentrations (*c.* 20–85 ng/g U, 5–95 percentile range). However, garnet lack visible inclusions (CL; Fig. 3), and counts of U and Zr (proxy for zircon and rutile), if displayed as a time series, are stable throughout ablation (Supplementary Figure S2). Therefore, U is likely lattice-bound at very low concentrations rather than in an unobserved included phase. Contamination of some ablations by ¹³⁷Ba (presumably from kimberlite groundmass) was encountered, and we have excluded those spots from age calculations. In spots considered to be 'uncontaminated' by kimberlite groundmass, a median of 15 CPS (background-corrected) of ¹³⁷Ba was measured. Spots were placed to avoid visible cracks (Fig. 3), but it is possible that excluded analyses encountered elongate areas of higher Back-scattered electron (BSE) response (Fig. 3) corresponding to contamination from kimberlite melt as the ablation pits were drilled.

Garnet major element compositions are uniform within each Bultfontein xenolith sample (BSK064; BP002; CLA13; CLA51). Equilibration temperatures were calculated to determine whether samples were likely open to diffusion during mantle residence, and therefore whether ages likely record kimberlite eruption. These were calculated using the empirical Ni-in-grt thermometer of Ryan *et al.* (1996). Our results indicate that harzburgite xenoliths from Bultfontein (BSK064; BP002; CLA51) were sampled from an extremely narrow temperature interval of 966 to 981 °C, in agreement with previously published results from garnet–orthopyroxene Fe–Mg cation exchange thermometry from sample BP002 (975 ± 17 °C; Tomlinson *et al.* 2018). A lherzolite xenolith from Bultfontein (CLA13) is derived from higher-temperature conditions, estimated at 1057 °C (Table 1). Note that these temperatures are most likely to represent conditions on the geotherm prior to entrainment in kimberlite melt.

4.a. Uranium–lead dating

Our U–Pb garnet age for the emplacement of the Bultfontein kimberlite is 84.0 ± 8.1 Ma. U–Pb dates of Bultfontein xenolith garnet are provided on Wetherill concordia in Figure 4. As ²³⁵U was not

independently measured, ages were calculated using Tera–Wasserburg ratios. Data are displayed on a Wetherill plot to make the analyses easier to observe. Four xenoliths were analysed. As all xenoliths provide age information that overlaps within uncertainty and are sampled from a domain above the likely closure temperature of the U–Pb system in pyrope, we consider all four xenoliths to represent a single sample, yielding a more precise overall emplacement age (Fig. 4). Individual concordia diagrams for each xenolith are provided in Supplementary Figure S3.

The initial ²⁰⁷Pb/²⁰⁶Pb ratio is 0.95 ± 0.10 (Fig. 4). Contrastingly, the ²⁰⁷Pb/²⁰⁶Pb ratio of the host kimberlite is 0.818 ± 0.002 (Kramers & Smith, 1983); kimberlite magmas in South Africa often have radiogenic compositions of common Pb attributed to part-sampling HIMU sources (Collerson *et al.* 2010), though with exceptions, such as the 1.15 Ga Premier pipe (Tappe *et al.* 2020). Regardless of the low precision of the initial ²⁰⁷Pb/²⁰⁶Pb ratio calculated for these garnet, the initial isotopic composition of common Pb in these xenolith garnet is not within error of the host kimberlite magma.

5. Discussion

5.a. Comparison of garnet ages to previous results

Our peridotitic pyrope garnet age of 84.0 ± 8.1 Ma for the emplacement of the (Group I) Bultfontein kimberlite is obtained despite extremely low concentrations of U (*c.* 20–85 ng/g). Sufficiently high ratios of U to common Pb in our samples, coupled with an analytical procedure that ablates vast quantities of material (130 μm spot size) with long dwell times to yield sufficient ions for analysis, permits their dating. This finding contradicts recent meta-analysis (*i.e.* analysis of aggregated data from several studies) of garnet that considered pyrope garnet and garnet from peridotites as poor candidates for U–Pb dating, based on low U concentrations (Deng *et al.* 2022). This may be explained, as the meta-analysis of Deng *et al.* (2022) did not account for high U/Pb, only considering the concentration of U. In most garnet in this study, a majority of Pb in the analysed crystals is radiogenic and many garnet analyses are near-concordant. This finding could fit with the

Table 2. Summary of analytical set-up for experiments, after Horstwood *et al.* (2016)

Laboratory and sample preparation	
Laboratory name	iCRAG Laboratory, Dept of Geology, Trinity College Dublin
Sample type/mineral	Pyrope-rich garnet in peridotitic mantle xenoliths from Bultfontein
Sample preparation	200 μm thick rock slices mounted on glass slides
Imaging	CL and BSE, Tescan TIGER MIRA3 Variable Pressure FE-SEM
Laser ablation system	
Make, model and type	Teledyne-Cetac Analyte Excite
Ablation cell and volume	HelEx 2-volume ablation cell; coupled to the ICPMS via an in-house adjustable-volume signal smoothing device
Laser wavelength (nm)	193 nm excimer laser
Pulse width (ns)	>5 ns
Fluence (J cm^{-2})	2.1 J cm^{-2}
Repetition rate (Hz)	10 Hz
Ablation duration (s)	40 s
Ablation pit depth / ablation rate	NA
Spot diameter (μm) nominal/actual	130 μm (circular spot)
Sampling mode/pattern	Static spot ablation
Carrier gas	100 % He in the cell, Ar make-up gas and N_2 added via a Y-piece
Cell carrier gas flow (L min^{-1})	0.56 L min^{-1}
ICP-MS instrument	
Make, model and type	Agilent Technologies 7900 quadrupole ICPMS
Sample introduction	Ablation aerosol
RF power (W)	1550 W
Make-up gas flow (L min^{-1})	Sourced from Agilent 7900, 0.55 L min^{-1}
Detection system	Dual-mode discrete dynode electron multiplier
Masses measured	27; 29; 43; 52; 55; 60; 137; 206; 207; 208; 232; and 238
Integration time per peak / dwell times (s)	0.05; 0.01; 0.005; 0.005; 0.01; 0.01; 0.01; 0.15; ;0.15; 0.02; 0.01; and 0.11
Total integration time per output (s)	0.522 (incl. dead time)
'Sensitivity' as useful yield (%; element)	0.01 % U ((#ions detected/#atoms sampled) * 100; Schaltegger <i>et al.</i> , 2015)
IC dead time (ns)	38 ns
Data processing	
Gas blank	15 s on-peak zero subtracted

(Continued)

Table 2. (Continued)

Calibration strategy	NIST614 primary standard. U–Pb correction factor obtained from Odikhincha garnet, then applied to the other garnet reference materials (Afrikanda, Dashkesan and Chikskii garnet)
Reference material info	NIST614 isotope ratios: Woodhead and Hergt (2000). Odikhincha and Afrikanda garnet: Salnikova <i>et al.</i> (2019). Dashkesan garnet: Stifeeva <i>et al.</i> (2019). Chikskii garnet: Salnikova <i>et al.</i> (2018); Mud Tank zircon: Black and Gulson (1978)
Data-processing package used/c	Agilent MassHunter 3.3; Iolite V3.5 for U–Pb data processing. laser-induced elemental fractionation (LIEF) corrected using an exponential spline fit in Iolite; assumes reference material and samples behave identically
Uncertainty level and propagation	Ages are quoted at 2 s absolute, propagation from Paton <i>et al.</i> (2011)
Quality control / Validation	Secondary reference materials listed above and in-text

partitioning data of Van Westrenen *et al.* (2001), who demonstrate that very pyrope-rich garnet should exhibit strong partitioning between U^{4+} (1.0 Å) and Sr^{2+} (1.32 Å) on the X-site of the pyrope lattice, which preferentially partitions smaller ions ($\text{Mg}^{2+} = 0.86$ Å). Pb^{2+} (i.e. common Pb) has an even larger and more incompatible radius (1.33 Å). Further study of partitioning of Pb and U in pyrope garnet is warranted.

Our obtained age (84.0 ± 8.1 Ma) for emplacement of the Bultfontein kimberlite agrees with ages determined from Rb–Sr phlogopite (84.0 ± 0.9 Ma, MSWD unavailable; Kramers & Smith, 1983) and U–Pb zircon from a peridotite xenolith (83.8 Ma, uncertainty and MSWD unreported; Davis, 1977). Our garnet age is at the younger end of the range reported from Rb–Sr on phlogopite from kimberlite (90 ± 3 Ma, MSWD unreported; Allsopp & Barret, 1975), and zircon (91.8 Ma, uncertainty and MSWD unreported; Davis, 1977).

5.b. Thermodynamic interpretation of garnet ages

We next consider whether the obtained garnet U–Pb dates reflect: (i) garnet formation, or (ii) freezing of the U–Pb system after eruption. Equilibrated textures in our granular peridotite samples (Fig. 2), depleted garnet compositions (high Cr; Table 1) and lack of trace element zoning (sample BP002; Tomlinson *et al.* 2018) are all accepted to be the result of long-term mantle residence (e.g. Harte, 1977). In addition, Lu–Hf dating of some comparable garnets from the Kimberley region yields Archaean ages (e.g. Branchetti *et al.* 2021). These features are consistent with an ancient formation age and long-term mantle residence. Younger (i.e. reset) two-point Sm–Nd and Lu–Hf isochron ages are also reported (from Cpx–Grt pairs) in the Kimberley region, but such grains have ancient Hf-isotope compositions consistent with ancient formation (Bedini *et al.* 2004). The second option is therefore much more likely; garnet are very old but record a Cretaceous age due to the rapid out-diffusion of Pb before kimberlite eruption.

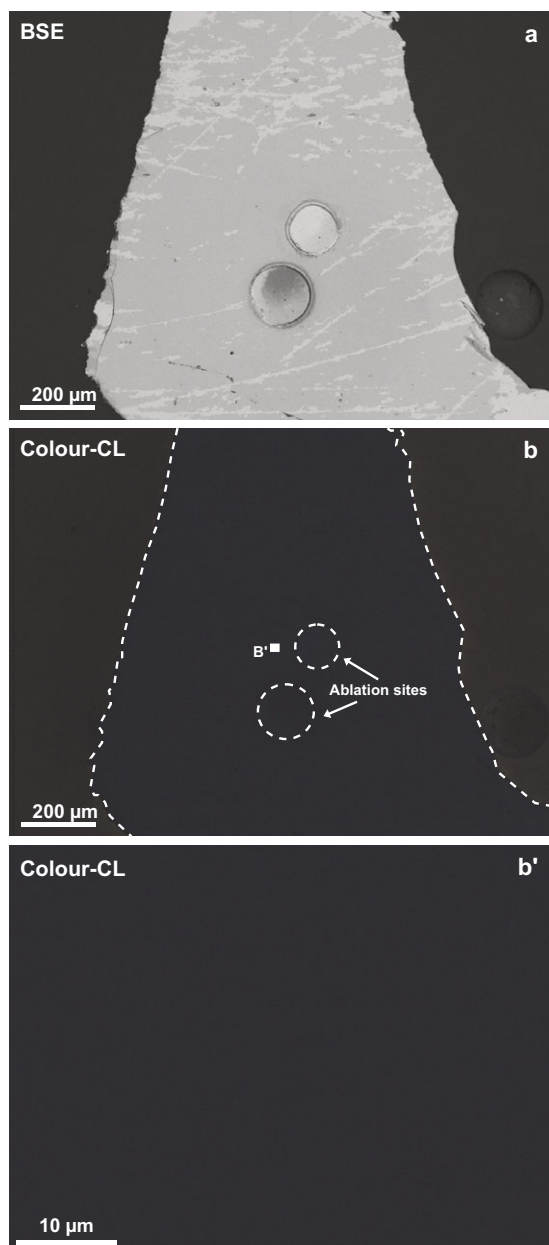


Fig. 3. (Colour online) Under BSE (a), mantle garnet are uniform except along linear features, corresponding to cracks. Garnet are featureless at any scale under CL (b); the grain analysed is highlighted by a dotted white outline. A selected tiny area (square in (b)) is shown in (b'). Garnet produce an extremely weak CL response. The point of these images containing few or no features is to demonstrate that no high-CL response regions corresponding to inclusions (e.g. zircon) are seen.

Given the above, Ni-thermometry data (Table 1) are interpreted to reflect the temperature of garnet equilibration in the lithosphere prior to entrainment in their host kimberlite. At $c. 966\text{--}1057^\circ\text{C}$, garnet are resident above the minimum proposed closure temperature of the pyrope–almandine U–Pb system ($\sim 800^\circ\text{C}$; Mezger *et al.* 1989). Most likely, Pb would have rapidly diffused out of garnet during potentially billions of years of residence in the mantle until the garnet U–Pb system cooled below its closure temperature, i.e. after emplacement on or near the Earth’s surface. This model is shown in Figure 5. We speculate that Pb may diffuse from garnet into pyroxene (particularly clinopyroxene) or grain boundary spaces during mantle residence at high T , though this has not been

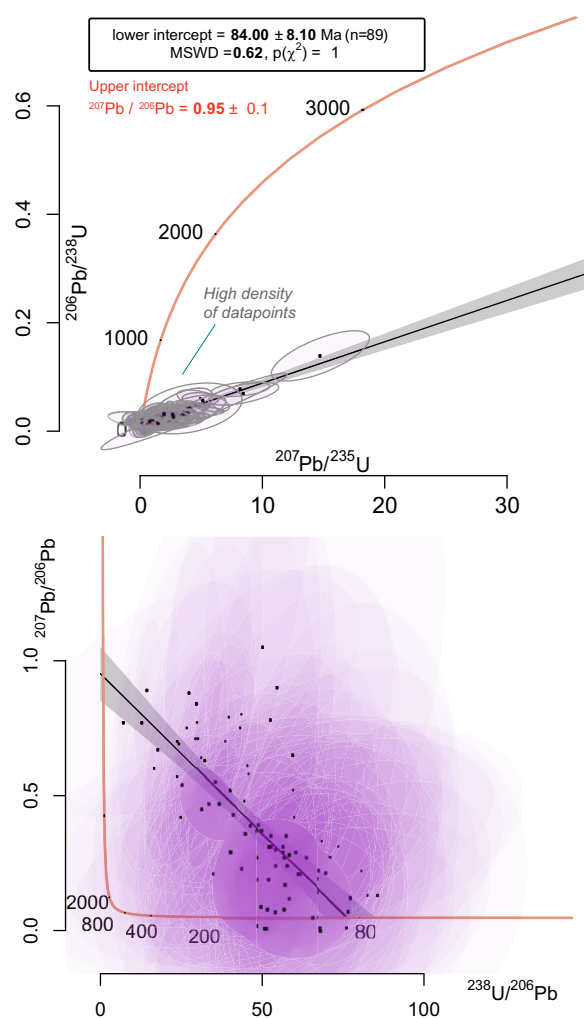


Fig. 4. (Colour online) $^{207}\text{Pb}/^{206}\text{Pb}$ vs $^{206}\text{Pb}/^{238}\text{U}$ garnet U–Pb discordia age of Bultfontein xenolith garnet. Age calculations employed the independently measured $^{207}\text{Pb}/^{206}\text{Pb}$ and $^{206}\text{Pb}/^{238}\text{U}$ ratios, but are here presented both in a Tera–Wasserburg diagram and transformed for display on Wetherill concordia for comparison. Ellipses are plotted at 2σ . In the Tera–Wasserburg diagram, ellipses are plotted with low transparency to show regions of greatest data density.

tested. Neither has the effect of grain size on diffusion been tested; the moderate precision of our analyses and the large spot sizes used preclude measurement of grain boundary effects. Within the precision of the analyses, the age population of pyrope-rich garnet from Bultfontein xenoliths is unimodal (i.e. $\text{MSWD} \sim 1$; see Fig. 4), indicating that grain-size effects must be relatively minor (at most on the order of a few Myr).

An alternative explanation for these ages, as being a product of recrystallization of garnet en route to the surface, is not a credible mechanism, as the garnets are from within texturally equilibrated peridotite xenoliths and have depleted, Cr-rich garnet compositions (Table 1), though our data cannot rule out an *earlier* pre-kimberlite metasomatic origin for these garnet (e.g. Chepurov *et al.* 2019). Additionally, whilst the $^{207}\text{Pb}/^{206}\text{Pb}$ of mantle xenoliths from the Kaapvaal (estimated from whole rock and clinopyroxene) are quite variable (0.77–0.90; Kramers, 1977; Walker *et al.*, 1989; Fitzpayne *et al.* 2020; Smart *et al.* 2021), kimberlite metasomatized mantle and kimberlites themselves generally cluster at the low end of this range (Kramers, 1977; Fitzpayne *et al.* 2020). This suggests

that the comparatively high initial $^{207}\text{Pb}/^{206}\text{Pb}$ composition of our xenolith garnet (Fig. 4) is unrelated to kimberlite metasomatism and also rules out garnet recrystallization during kimberlite magmatism as a viable explanation for their isotopic character.

5.c. Potential applications of U–Pb dating for pyrope garnet

Pyrope-rich peridotitic garnet are common in the cratonic lithospheric mantle (5–10% modal abundance in garnet-bearing xenoliths), easy to differentiate from crustal garnet by colour, and are big (~0.5 cm diameter) and resistant to surface weathering, if not to metasomatic alteration (kelyphite alteration). Peridotitic garnet is already used to track mineral detritus derived from kimberlite provinces (e.g. Grütter *et al.* 2004; Shchukina & Shchukin, 2018). Using our methodology (with further refinement), it may be possible to go further and to identify *specific* kimberlite fields by their U–Pb dates. U–Pb dating of peridotitic garnet may thus constitute a useful mining vector in diamond exploration. In addition, U–Pb dating from mineral detritus could be used to identify episodes of kimberlite magmatism in less studied regions (e.g. South American kimberlites); or to shed light on the history of pre-Phanerozoic kimberlite magmatism – particularly for Archaean diamond placers for which the primary kimberlite sources are elusive (e.g. Stachel *et al.* 2006; Smart *et al.* 2016).

It is possible that U–Pb dates from pyrope-rich garnet may not always characterize emplacement ages. Depending on the thermal conditions of the lithosphere since its formation, garnet resident at lower ambient mantle temperatures (<800°C, presumably at shallower mantle depths) may preserve older ages. In this instance, double- or triple-dating on peridotitic garnet might reveal both the formation and later metasomatism of the Earth's subcontinental lithospheric mantle if, for example, there were differences in the U–Pb, Sm–Nd and/or Lu–Hf dates in individual samples (e.g. Bedini *et al.* 2004). Use of triple-quadrupole or multi-collector ICPMS or SIMS may improve sensitivity or increase the number of isotopic techniques applicable, and thus broaden the scope and applicability of the method. The collection of TIMS data from suitable pyrope-rich garnet to generate low-U pyrope-rich garnet standards is also desirable (cf. Chen *et al.* 2021).

Lastly, with modifications to our method (perhaps use of more sensitive multi-collector/sector field ICPMS or SIMS), it may be possible to obtain entrapment ages for peridotitic garnet inclusions in diamond. Sufficiently precise U–Pb dating could be applied to pyrope-rich garnet inclusions in diamond, not to date emplacement, but instead to date inclusion entrapment and therefore periods of diamond growth. While obtaining individual garnet ages using our method is untested and will require further method development, it is an attractive prospect given that peridotitic garnet is the most common diamond inclusion type in peridotitic diamonds (Stachel & Harris, 2008).

One obstacle may be inclusion size. Monomineralic inclusions in diamond range from 10 to 200 µm in size (Meyer & Boyd, 1972). The authors are unaware of studies specifically detailing the average size of pyrope-rich garnet inclusions in diamond. However, there are published examples of relatively large pyrope-rich garnet inclusions with long-axes *c.* 100–125 µm (Logvinova *et al.* 2005) and even up to *c.* 250 µm (e.g. Wang *et al.* 1991). Thus, while a method requiring a large beam width may be better suited to the analysis of large inclusions, there are natural diamond inclusions in a size range that may be analysed using an unmodified version of our analytical procedure by LA-Q-ICPMS. Additionally, as the limiting factor on the precision of our method

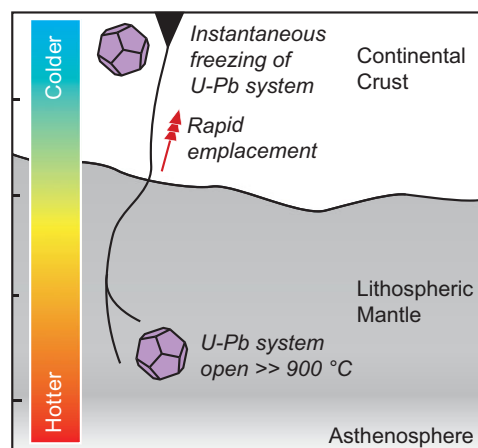


Fig. 5. (Colour online) Conceptual model of the behaviour of the U–Pb system in pyrope-rich garnet from sampled xenoliths. Garnet sampled from very high temperatures, as in this study, will reflect emplacement. Garnet yielding lower equilibration temperatures or encapsulated in diamond (none in this study) might retain ancient information.

is measurement of sufficient radiogenic Pb, older materials, such as pyrope inclusions in cratonic diamonds, should yield much more precise single-grain U–Pb ages than the ‘young’ (80 Ma) pyrope analysed in this study (assuming similar initial concentrations of U).

Comparatively, existing methods for the isotopic dating of individual silicate inclusions in diamonds are largely non-existent or cannot be undertaken *in situ* (cf. Koornneef *et al.* 2017). Rather, in the past published ages were typically obtained on pooled samples (e.g. Richardson *et al.* 1984) comprising tens to hundreds of inclusions and thus may represent mixed ages.

6. Conclusions

- It is possible to obtain U–Pb dates from extremely U-poor (20–85 ng/g) pyrope garnet in mantle xenoliths. Our garnet yield emplacement ages for entraining kimberlite magmas, as garnet from peridotite xenoliths in Kimberley are likely resident above the closure temperature of the garnet U–Pb system in local ambient lithospheric mantle conditions.
- Our procedure employs TIMS-dated garnet standards and very large laser ablation spots (130 µm diameter). Despite low U concentrations, the ratio of radiogenic to common Pb in peridotitic garnet is very high, which permits dating.
- Our method also provides information on the initial $^{207}\text{Pb}/^{206}\text{Pb}$ isotopic compositions of the garnet (0.95 ± 0.10), which are significantly less radiogenic than the Pb-isotopic composition of the host kimberlite (0.818 ± 0.002); upper-intercept ratios are similar to clinopyroxene in mantle xenoliths from other diatremes on the Kaapvaal Craton. Therefore, the U–Pb approach may, in future, be used to investigate spatial or temporal variation in Pb–Pb isotope composition and to better understand the origin of metasomatic fluids and melts.
- Eclogitic garnet from Jagersfontein could not be dated, as the concentrations of U (*c.* 8 ng/g) were too low to determine U–Pb ratios using our approach, which employed quadrupole ICPMS. Peridotitic garnet may be a better target for dating than eclogitic garnet. Pyrope-rich peridotitic garnets are easily distinguished by their diagnostic purple colour.

- Potential applications of pyrope U–Pb dating may include its use as a detrital kimberlite exploration tool, especially for weathered-out pipes, or to provide diamond-entrapment ages. The method could also be applied to any igneous rock containing pyrope garnet xenoliths/xenocrysts.

Supplementary material. To view supplementary material for this article, please visit <https://doi.org/10.1017/S0016756823000122>

Acknowledgements. The authors would like to thank Paul Guyett and Cora McKenna for their assistance during analysis and maintenance of lab facilities to an exceptional standard; Clare Stead and Balz S. Kamber for providing the sample materials and additionally for several productive conversations; and David M. Chew for helping us to develop our ideas. GJO'S thanks J. Stephen Daly for his mentorship. The authors are appreciative of two anonymous reviews and one identified review by Sebastian Tappe, which greatly improved the manuscript. We thank the editor, Sarah Sherlock, for sourcing these expert and insightful reviewers.

Financial support. This project has received support from two Irish Research Council grants: a *Government of Ireland Postdoctoral Fellowship* held by GJO'S (GOIPD/2019/906), and a *Government of Ireland Postgraduate Scholarship* held by BCH (GOIPG/2017/1132). CM is supported by a *Starting Investigator Research Grant* from Science Foundation Ireland (18/SIRG/5559). The iCRAG geochronology facility is supported by SFI award 13/RC/2092.

Conflicts of interest. None.

References

- Allsopp HL and Barrett DR (1975) Rb/Sr age determinations on South African kimberlite pipes. *Physics and Chemistry of the Earth* **9**, 605–17. doi: [10.1016/0079-1946\(75\)90041-5](https://doi.org/10.1016/0079-1946(75)90041-5)
- Bedini RM, Blichert-Toft J, Boyet M and Albarede F (2004) Isotopic constraints on the cooling of the continental lithosphere. *Earth and Planetary Science Letters* **223**, 99–111. doi: [10.1016/j.epsl.2004.04.012](https://doi.org/10.1016/j.epsl.2004.04.012)
- Black LP and Gulson BL (1978) The age of the Mud Tank carbonatite, Strangways Range, Northern Territory. *BMR Journal of Australian Geology and Geophysics* **3**, 227–32.
- Branchetti M, Zepper JC, Peters ST, Koornneef JM and Davies GR (2021) Multi-stage garnet formation and destruction in Kimberley harzburgitic xenoliths, South Africa. *Lithos* **390**, 106119. doi: [10.1016/j.lithos.2021.106119](https://doi.org/10.1016/j.lithos.2021.106119)
- Chen YH, Hu RZ, Lan TG, Wang H, Tang YW, Yang YH, Tian ZD and Ulrich T (2021) Precise U–Pb dating of grandite garnets by LA-ICP-MS: assessing ablation behaviors under matrix-matched and non-matrix-matched conditions and applications to various skarn deposits. *Chemical Geology* **572**, 120198. doi: [10.1016/j.chemgeo.2021.120198](https://doi.org/10.1016/j.chemgeo.2021.120198)
- Chepurov AA, Faryad SW, Agashev AM, Strnad L, Jedlicka R, Turkin AI, Mihaljevic M and Lin VV (2019) Experimental crystallization of a subcalcic Cr-rich pyrope in the presence of REE-bearing carbonatite. *Chemical Geology* **509**, 103–14. doi: [10.1016/j.chemgeo.2019.01.011](https://doi.org/10.1016/j.chemgeo.2019.01.011)
- Collerson KD, Williams Q, Ewart AE and Murphy DT (2010) Origin of HIMU and EM-1 domains sampled by ocean island basalts, kimberlites and carbonatites: the role of CO₂-fluxed lower mantle melting in thermochemical upwellings. *Physics of the Earth and Planetary Interiors* **181**, 112–31. doi: [10.1016/j.pepi.2010.05.008](https://doi.org/10.1016/j.pepi.2010.05.008)
- Davis CL (1977) The ages and uranium contents of zircons from kimberlites and associated rocks. *Carnegie Institution of Washington Yearbook* **76**, 631–54.
- Deng Y, Zhong R, Li D, Li Y and Cui H (2022) Hunting the datable garnet by LA-ICP-MS U–Pb method: predicting garnet U concentration based on major and minor elements. *Acta Geologica Sinica – English Ed.* Published online 12 March 2022. doi: [10.1111/1755-6724.14921](https://doi.org/10.1111/1755-6724.14921)
- DeWolf CP, Zeissler CJ, Halliday AN, Mezger K and Essene EJ (1996) The role of inclusions in U–Pb and Sm–Nd garnet geochronology: stepwise dissolution experiments and trace uranium mapping by fission track analysis. *Geochimica et Cosmochimica Acta* **60**, 121–34. doi: [10.1016/0016-7037\(95\)00367-3](https://doi.org/10.1016/0016-7037(95)00367-3)
- Fiorentini ML, O'Neill C, Giuliani A, Choi E, Maas R, Pirajno F and Foley S (2020) Bushveld superplume drove Proterozoic magmatism and metallogenesis in Australia. *Scientific Reports* **10**, 1–10. doi: [10.1038/s41598-020-76800-0](https://doi.org/10.1038/s41598-020-76800-0)
- Fitzpayne A, Giuliani A, Hergt J, Woodhead JD and Maas R (2020) Isotopic analyses of clinopyroxenes demonstrate the effects of kimberlite melt metasomatism upon the lithospheric mantle. *Lithos* **370–371**, 105595. doi: [10.1016/j.lithos.2020.105595](https://doi.org/10.1016/j.lithos.2020.105595)
- Galuskina IO, Galuskin EV, Armbruster T, Lazic B, Kusz J, Dzierzanowski P, Gazeev VM, Pertsev NN, Prusik K, Zadov AE and Winiarski A (2010) Elbrusite-(Zr)—A new uranian garnet from the Upper Chegem caldera, Kabardino-Balkaria, Northern Caucasus, Russia. *American Mineralogist* **95**, 1172–81.
- Griffin WL, Batumike JM, Greau Y, Pearson NJ, Shee SR and O'Reilly SY (2014) Emplacement ages and sources of kimberlites and related rocks in southern Africa: U–Pb ages and Sr–Nd isotopes of groundmass perovskite. *Contributions to Mineralogy and Petrology* **168**, 1–13. doi: [10.1007/s00410-014-1032-4](https://doi.org/10.1007/s00410-014-1032-4)
- Griffin WL, O'Reilly SY, Natapov LM and Ryan CG (2003) The evolution of lithospheric mantle beneath the Kalahari Craton and its margins. *Lithos* **71**, 215–41. doi: [10.1016/j.lithos.2003.07.006](https://doi.org/10.1016/j.lithos.2003.07.006)
- Grütter HS, Gurney JJ, Menzies AH and Winter F (2004) An updated classification scheme for mantle-derived garnet, for use by diamond explorers. *Lithos* **77**, 841–57. doi: [10.1016/j.lithos.2004.04.012](https://doi.org/10.1016/j.lithos.2004.04.012)
- Harte B (1977) Rock nomenclature with particular relation to deformation and recrystallisation textures in olivine-bearing xenoliths. *The Journal of Geology* **85**, 279–88. doi: [10.1086/628299](https://doi.org/10.1086/628299)
- Heaman LM, Phillips D and Pearson G (2019) Dating kimberlites: methods and emplacement patterns through time. *Elements* **15**, 399–404. doi: [10.2138/gselements.15.6.399](https://doi.org/10.2138/gselements.15.6.399)
- Hoare BC, Sullivan GO and Tomlinson EL (2021) Metasomatism of the Kaapvaal Craton during Cretaceous intraplate magmatism revealed by combined zircon U–Pb isotope and trace element analysis. *Chemical Geology* **578**, 120302. doi: [10.1016/j.chemgeo.2021.120302](https://doi.org/10.1016/j.chemgeo.2021.120302)
- Horstwood MS, Košler J, Gehrels G, Jackson SE, McLean NM, Paton C, Pearson NJ, Sircombe K, Sylvester P, Vermeesch P and Bowring JF (2016) Community-derived standards for LA-ICP-MS U–(Th–) Pb geochronology: uncertainty propagation, age interpretation and data reporting. *Geostandards and Geoanalytical Research* **40**, 311–32.
- Janney PE, Shirey SB, Carlson RW, Pearson DG, Bell DR, le Roex AP, Ishikawa A, Nixon PH and Boyd FR (2010) Age, composition and thermal characteristics of South African off-craton mantle lithosphere: evidence for a multi-stage history. *Journal of Petrology* **51**, 1849–90. doi: [10.1093/ptrology/egq041](https://doi.org/10.1093/ptrology/egq041)
- Jochum KP, Willbold M, Raczek I, Stoll B and Herwig K (2005) Chemical characterisation of the USGS reference glasses GSA-1G, GSC-1G, GSD-1G, GSE-1G, BCR-2G, BHVO-2G and BIR-1G using EPMA, ID-TIMS, ID-ICP-MS and LA-ICP-MS. *Geostandards and Geoanalytical Research* **29**, 285–302. doi: [10.1111/j.1751-908x.2005.tb00901.x](https://doi.org/10.1111/j.1751-908x.2005.tb00901.x)
- Jung S and Mezger K (2003) U–Pb garnet chronometry in high-grade rocks: case studies from the central Damara orogen (Namibia) and implications for the interpretation of Sm–Nd garnet ages and the role of high U–Th inclusions. *Contributions to Mineralogy and Petrology* **146**, 382–96. doi: [10.1007/s00410-003-0506-6](https://doi.org/10.1007/s00410-003-0506-6)
- Kinny PD, Compston W, Bristow JW and Williams IS (1989) Archean mantle xenocrysts in a Permian kimberlite: two generations of kimberlitic zircon in Jwaneng DK2, southern Botswana. In *Proceedings of the Fourth International Kimberlite Conference, vol. 2: Kimberlites and Related Rocks* (ed J Ross), pp. 833–42. Blackwell, Melbourne, Australia: Geological Society of Australia Special Publication no. 14.
- Koornneef JM, Gress MU, Chinn IL, Jelsma HA, Harris JW and Davies GR (2017) Archean and Proterozoic diamond growth from contrasting styles of large-scale magmatism. *Nature Communications* **8**, 648.
- Kramers JD (1977) Lead and strontium isotopes in Cretaceous kimberlites and mantle-derived xenoliths from southern Africa. *Earth and Planetary Science Letters* **34**, 419–31. doi: [10.1016/0012-821X\(77\)90053-X](https://doi.org/10.1016/0012-821X(77)90053-X)
- Kramers JD and Smith CB (1983) A feasibility study of U–Pb and Pb–Pb dating of kimberlites using groundmass mineral fractions and whole-rock samples. *Chemical Geology* **41**, 23–38. doi: [10.1016/S0009-2541\(83\)80003-5](https://doi.org/10.1016/S0009-2541(83)80003-5)

- Li D, Wu Z, Sun X, Shuai S and Fu Y (2022) Emplacement ages of diamondiferous kimberlites in the Wafangdian District, North China Craton: new evidence from LA-ICP-MS U-Pb geochronology of andradite-rich garnet. *Gondwana Research* **109**, 493–517. doi: [10.1016/j.gr.2022.05.016](https://doi.org/10.1016/j.gr.2022.05.016)
- Logvinova AM, Taylor LA, Floss C and Sobolev NV (2005) Geochemistry of multiple diamond inclusions of harzburgitic garnets as examined in situ. *International Geology Review* **47**, 1223–33.
- Meyer HOA and Boyd FR (1972) Composition and origin of crystalline inclusions in natural diamonds. *Geochimica et Cosmochimica Acta* **36**, 1255–73.
- Mezger K, Hanson GN and Bohlen SR (1989) U–Pb systematics of garnet: dating the growth of garnet in the late Archean Pikwitonei granulite domain at Cauchon and Natawahunan Lakes, Manitoba, Canada. *Contributions to Mineralogy and Petrology* **101**, 136–48. doi: [10.1007/BF00375301](https://doi.org/10.1007/BF00375301)
- Mitchell RH (1995) *Kimberlites, Orangeites, and Related Rocks*. Boston, MA: Springer. doi: [10.1007/978-1-4615-1993-5_1](https://doi.org/10.1007/978-1-4615-1993-5_1)
- Morton AC and Hallsworth C (2007) Stability of detrital heavy minerals during Burial diagenesis. In *Developments in Sedimentology*, vol. 58 (eds M Mange and D Wright), pp. 215–45. Amsterdam: Elsevier. doi: [10.1016/S0070-4571\(07\)58007-6](https://doi.org/10.1016/S0070-4571(07)58007-6)
- Noyes A, Heaman L and Creaser R (2011) A comparison of chronometers applied to monastery kimberlite and the feasibility of U–Pb ilmenite geochronology. In *Dyke Swarms: Keys for Geodynamic Interpretation* (ed R Srivastava). Berlin and Heidelberg: Springer. doi: [10.1007/978-3-642-12496-9_25](https://doi.org/10.1007/978-3-642-12496-9_25)
- Paton C, Hellstrom J, Paul B, Woodhead J and Hergt J (2011) Iolite: freeware for the visualisation and processing of mass spectrometric data. *Journal of Analytical Atomic Spectrometry* **26**, 2508–18. doi: [10.1039/c1ja10172b](https://doi.org/10.1039/c1ja10172b)
- Petrus JA and Kamber BS (2012) VizualAge: a novel approach to laser ablation ICP-MS U–Pb geochronology data reduction. *Geostandards and Geoanalytical Research* **36**, 247–70. doi: [10.1111/j.1751-908X.2012.00158.x](https://doi.org/10.1111/j.1751-908X.2012.00158.x)
- Philips D, Clarke W and Jaques AL (2012) New ⁴⁰Ar/³⁹Ar ages for the West Kimberley lamproites and implications for Australian Plate geodynamics. International Kimberlite Conference Abstracts, 39–41.
- Rák Z, Ewing RC and Becker U (2011) Role of iron in the incorporation of uranium in ferric garnet matrices. *Physical Review B* **84**, 155128. doi: [10.1103/PhysRevB.83.155123](https://doi.org/10.1103/PhysRevB.83.155123)
- Reich M, Ewing RC, Ehlers TA and Becker U (2007) Low-temperature anisotropic diffusion of helium in zircon: implications for zircon (U–Th)/He thermochronometry. *Geochimica et Cosmochimica Acta* **71**, 3119–30. doi: [10.1016/j.gca.2007.03.033](https://doi.org/10.1016/j.gca.2007.03.033)
- Richardson SH, Gurney JJ, Erlank AJ and Harris J (1984) Origin of diamonds in old enriched mantle. *Nature* **310**, 198–202.
- Ryan G, Griffin WL and Pearson NJ (1996) Garnet geotherms: pressure-temperature data from Cr–pyrope garnet xenocrysts in volcanic rocks. *Journal of Geophysical Research: Solid Earth* **101**, 5611–25. doi: [10.1029/95JB03207](https://doi.org/10.1029/95JB03207)
- Salnikova EB, Chakhmouradian AR, Stifeeva MV, Reguir EP, Kotov AB, Gritsenko YD and Nikiforov AV (2019) Calcic garnets as a geochronological and petrogenetic tool applicable to a wide variety of rocks. *Lithos* **338–339**, 141–54. doi: [10.1016/j.lithos.2019.03.032](https://doi.org/10.1016/j.lithos.2019.03.032)
- Salnikova EB, Stifeeva MV, Nikiforov AV, Yarmolyuk VV, Kotov AB, Anisimova IV, Sugorakova AM and Vrublevskii VV (2018) Andradite–morimotoite garnets as promising U–Pb geochronometers for dating ultrabasic alkaline rocks. *Doklady Earth Sciences* **480**, 778–82. doi: [10.1134/S1028334X18060168](https://doi.org/10.1134/S1028334X18060168)
- Sarkar C, Heaman LM and Pearson DG (2015) Duration and periodicity of kimberlite volcanic activity in the Lac de Gras kimberlite field, Canada and some recommendations for kimberlite geochronology. *Lithos* **218–219**, 155–66. doi: [10.1016/j.lithos.2015.01.017](https://doi.org/10.1016/j.lithos.2015.01.017)
- Schaltegger U, Schmitt AK and Horstwood MSA (2015) U–Th–Pb zircon geochronology by ID-TIMS, SIMS, and laser ablation ICP-MS: Recipes, interpretations, and opportunities. *Chemical Geology* **402**, 89–110.
- Seman S, Stockli DF and McLean NM (2017) U–Pb geochronology of grossular–andradite garnet. *Chemical Geology* **460**, 106–16. doi: [10.1016/j.chemgeo.2017.04.020](https://doi.org/10.1016/j.chemgeo.2017.04.020)
- Shchukina EV and Shchukin VS (2018) Diamond exploration potential of the northern East European platform. *Minerals* **8**, 1–17. doi: [10.3390/min8050189](https://doi.org/10.3390/min8050189)
- Smart KA, Tappe S, Stern RA, Webb SJ and Ashwal LD (2016) A review of the isotopic and trace element evidence for mantle and crustal processes in the Hadean and Archean: implications for the onset of plate tectonic subduction. *Nature Geoscience* **9**, 255–9.
- Smart KA, Tappe S, Woodland AB, Harris C, Corcoran L and Simonetti A (2021) Metasomatized eclogite xenoliths from the central Kaapvaal craton as probes of a seismic mid-lithospheric discontinuity. *Chemical Geology* **578**, 120286. doi: [10.1016/j.chemgeo.2021.120286](https://doi.org/10.1016/j.chemgeo.2021.120286)
- Smith CB, Allsopp HL, Kramers JD, Hutchinson G and Roddick JC (1985) Emplacement ages of Jurassic–Cretaceous South African kimberlites by the Rb–Sr method on phlogopite and whole-rock samples. *Transactions of the Geological Society of South Africa* **88**, 249–66.
- Stachel T, Banas A, Muehlenbachs K, Kurszlaukis S and Walker EC (2006) Archean diamonds from Wawa (Canada): samples from deep cratonic roots predating cratonization of the Superior Province. *Contributions to Mineralogy and Petrology* **151**, 737–50. doi: [10.1007/s00410-006-0090-7](https://doi.org/10.1007/s00410-006-0090-7)
- Stachel T and Harris JW (2008) The origin of cratonic diamonds: constraints from mineral inclusions. *Ore Geology Reviews* **34**, 5–32. doi: [10.1016/j.oregeorev.2007.05.002](https://doi.org/10.1016/j.oregeorev.2007.05.002)
- Stanley JR and Flowers RM (2016) Dating kimberlite emplacement with zircon and perovskite (U–Th)/He geochronology. *Geochemistry, Geophysics, Geosystems* **17**, 4517–33. doi: [10.1002/2016GC006519](https://doi.org/10.1002/2016GC006519)
- Stifeeva MV, Salnikova EB, Samsonov AV, Kotov AB and Gritsenko YD (2019) Garnet U–Pb age of skarns from Dashkesan deposit (Lesser Caucasus). *Doklady Earth Sciences* **487**, 953–6. doi: [10.1134/S1028334X19080178](https://doi.org/10.1134/S1028334X19080178)
- Sun J, Tappe S, Kostrovitsky SI, Liu CZ, Skuzovatov SY and Wu FY (2018) Mantle sources of kimberlites through time: a U–Pb and Lu–Hf isotope study of zircon megacrysts from the Siberian diamond fields. *Chemical Geology* **479**, 228–40. doi: [10.1016/j.chemgeo.2018.01.013](https://doi.org/10.1016/j.chemgeo.2018.01.013)
- Tappe S, Dongre A, Liu CZ and Wu FY (2018a) ‘Premier’ evidence for prolonged kimberlite pipe formation and its influence on diamond transport from deep Earth. *Geology* **46**, 843–6. doi: doi.org/10.1130/G45097.1
- Tappe S, Kjarsgaard BA, Kurszlaukis S, Nowell GM and Phillips D (2014) Petrology and Nd–Hf isotope geochemistry of the Neoproterozoic Amon kimberlite sills, Baffin Island (Canada): evidence for deep mantle magmatic activity linked to supercontinent cycles. *Journal of Petrology* **55**, 2003–42. doi: [10.1093/ptrology/egu048](https://doi.org/10.1093/ptrology/egu048)
- Tappe S, Shaikh AM, Wilson AH and Stracke A (2022) Evolution of ultrapotassic volcanism on the Kaapvaal craton: deepening the orangeite versus lamproite debate. *Geological Society* **513**, 17–44.
- Tappe S and Simonetti A (2012) Combined U–Pb geochronology and Sr–Nd isotope analysis of the Ice River perovskite standard, with implications for kimberlite and alkaline rock petrogenesis. *Chemical Geology* **304–305**, 10–17. doi: [10.1016/j.chemgeo.2012.01.030](https://doi.org/10.1016/j.chemgeo.2012.01.030)
- Tappe S, Smart K, Torsvik T, Massuyeau M and de Wit M (2018b) Geodynamics of kimberlites on a cooling Earth: clues to plate tectonic evolution and deep volatile cycles. *Earth and Planetary Science Letters* **484**, 1–14. doi: [10.1016/j.epsl.2017.72.013](https://doi.org/10.1016/j.epsl.2017.72.013)
- Tappe S, Stracke A, van Acken D, Strauss H and Luguet A (2020) Origins of kimberlites and carbonatites during continental collision: insights beyond decoupled Nd–Hf isotopes. *Earth-Science Reviews* **208**, 103287. doi: [10.1016/j.earscirev.2020.103287](https://doi.org/10.1016/j.earscirev.2020.103287)
- Tomlinson EL, Kamber BS, Hoare BC, Stead CV and Ildefonse B (2018) An exsolution origin for Archean mantle garnet. *Geology* **46**, 123–6. doi: [10.1130/G39680.1](https://doi.org/10.1130/G39680.1)
- Van Westrenen W, Blundy JD and Wood BJ (2001) High field strength element/rare earth element fractionation during partial melting in the presence of garnet: implications for identification of mantle heterogeneities. *Geochemistry, Geophysics, Geosystems* **2**, 1039.
- Vermeesch P (2018) IsoplotR: a free and open toolbox for geochronology. *Geoscience Frontiers* **9**, 1479–93. doi: [10.1016/j.gsf.2018.04.001](https://doi.org/10.1016/j.gsf.2018.04.001)

- Walker RJ, Carlson RW, Shirey SB and Boyd FR** (1989) Os, Sr, Nd, and Pb isotope systematics of southern African peridotite xenoliths: implications for the chemical evolution of subcontinental mantle. *Geochimica et Cosmochimica Acta* **53**, 1583–1595.
- Wang A, Wang W and Zhang A** (1991) Microstructural variations of a pyrope inclusion in diamond, as revealed by a micro-Raman spectroscopic study. *The Canadian Mineralogist* **29**, 517–24.
- Woodhead JD and Hergt JM** (2000) Pb-isotope analyses of USGS reference materials. *Geostandards Newsletter* **24**, 33–8. doi: [10.1111/j.1751-908X.2000.tb00584.x](https://doi.org/10.1111/j.1751-908X.2000.tb00584.x)
- Zartman RE and Richardson SH** (2005) Evidence from kimberlitic zircon for a decreasing mantle Th/U since the Archean. *Chemical Geology* **220**, 263–83. doi: [10.1016/j.chemgeo.2005.04.003](https://doi.org/10.1016/j.chemgeo.2005.04.003)